THE JOURNAL OF PHYSICAL CHEMISTRY B

Article

pubs.acs.org/JPCB

Proton Hopping and Long-Range Transport in the Protic Ionic Liquid [Im][TFSI], Probed by Pulsed-Field Gradient NMR and Quasi-Elastic Neutron Scattering

Megan L. Hoarfrost,*[,†,‡] Madhusudan Tyagi,[§,⊥] Rachel A. Segalman,[†,@] and Jeffrey A. Reimer[†,‡]

[†]Department of Chemical and Biomolecular Engineering, University of California, Berkeley, Berkeley, California 94720, United States

[‡]Energy and Environmental Technologies Division, Lawrence Berkeley National Laboratory, Berkeley, California 94720, United States

[§]National Institue of Standards and Technology Center for Neutron Research, Gaithersburg, Maryland 20899, United States

[⊥]Department of Materials Science and Engineering, University of Maryland, College Park, Maryland 20742, United States

[@]Materials Sciences Division, Lawrence Berkeley National Laboratory, Berkeley, California 94720, United States

Supporting Information

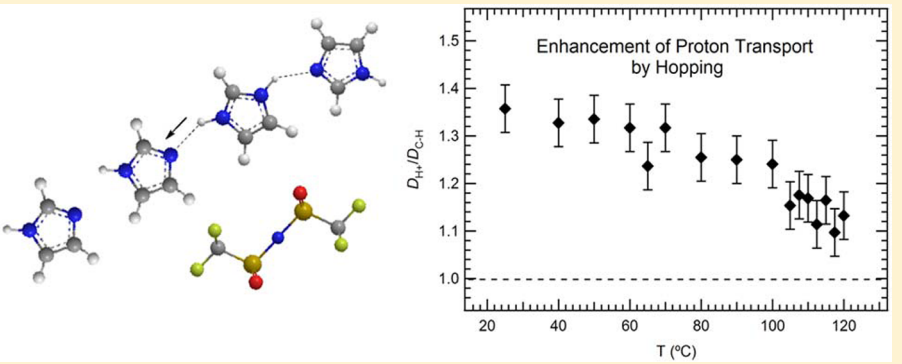

ABSTRACT: The management of proton conductivity in the protic ionic liquid imidazolium bis(trifluoromethylsulfonyl)imide ([Im][TFSI]) is investigated via the use of quasi-elastic neutron scattering (QENS) and pulsed-field gradient NMR. The introduction of excess neutral imidazole to [Im][TFSI] leads to enhanced conductivity. We find that proton dynamics in [Im][TFSI] with excess imidazole are characterized by proton hopping that is encompassed in the slower of two translational processes, as identified by QENS. This relatively slow process contributes to long-range diffusion more than the faster process. NMR diffusion measurements show that proton hopping decreases with increasing temperature, but significant proton hopping persists even at the maximum experimental temperature of 120 °C. This, in combination with minimal ion aggregation, leads to high proton conductivity and a high proton transference number over a wide temperature range.

INTRODUCTION

Protic ionic liquids are characterized by proton conductivity, negligible volatility, and good thermal and electrochemical stability. These features make them promising candidates for a wide variety of electrochemical applications, particularly those which operate at elevated temperatures (i.e., above the boiling point of water).[1] Systematic management of the proton conductivity in these ionic liquids is an important goal for many technologies, yet the scientific underpinnings for such management warrant further attention, in particular the relationship between ionic liquid composition and the atomistic mechanism by which protons move. For example, proton conductivity in imidazolium bis(trifluoromethylsulfonyl)imide ([Im][TFSI]) is known to be enhanced when it is prepared with an excess of imidazole.[2] In this scenario, proton hopping between hydrogen-bonded imidazole molecules is facilitated, where the excess imidazole fulfills the role of proton acceptor.[2−4] Proton hopping is presumed to decouple proton transport from molecular diffusion, leading to a high proton transference number, defined as the fraction of the current carried by the movement of acidic protons, in addition to overall faster proton conductivity.[5] A high proton transference number is desirable for applications such as proton exchange membrane fuel cells, as well as actuator applications that require asymmetric charge transport. We submit that a greater understanding of the mechanism of proton hopping in crafted imidazole-based ionic liquids will facilitate their use as electrolytes in these applications.

It has been understood for decades that imidazole molecules shuttle protons through biological membranes.[6] The observa-

Received: May 7, 2012
Revised: June 20, 2012
Published: June 26, 2012

dx.doi.org/10.1021/jp3044237 | J. Phys. Chem. B 2012, 116, 8201−8209

tion of enhanced acidic proton diffusion coefficients in imidazole/acid mixtures[3] was the first demonstration that imidazole facilitates fast proton hopping in an electrolyte. Since that demonstration, several theoretical studies have shed light on the details of the proton hopping mechanism in imidazole.[4,7−10] These studies have mapped out the predicted hydrogen bond network and intermolecular distances and shown that proton hopping involves two steps: a fast proton transfer step and a slow, rate-limiting reorientation step. These simulations are computationally demanding, and only recently has a simulation been performed using long enough time scales and a sufficient number of molecules to observe multiple hopping events.[7] The reorientation time scale was calculated to be ca. 20 ps, and the hop rate was calculated to be 1/36 ps^{-1}, the latter of which appears consistent with bulk-transport measurements.[3] Solid state nuclear magnetic resonance (NMR) experiments have observed imidazole ring flipping and quantified the activation energy to be similar to that of proton conductivity, confirming that ring flipping is an important part of the reorientation step.[11−13]

Direct experimental probes are desired to improve our understanding of proton hopping in imidazole and its relationship to macroscopic proton conductivity. Using NMR to measure self-diffusion is an invaluable tool for quantifying the amount of proton hopping and determining the proton transference number. For example, by comparison of the diffusion coefficients of acidic protons to the diffusion coefficients of protons covalently bound to the carbon atoms on imidazole in [Im][TFSI], it has been shown that proton hopping increases acidic proton diffusion by a factor of 1.4 at 30 °C when the ratio of imidazole to HTFSI is 4:1.[2] Furthermore, comparing proton diffusion to anion diffusion revealed that the proton transference number reaches 0.69 at this temperature and composition.[2] Quasi-elastic neutron scattering (QENS) has provided more detailed information about proton dynamics in protic and aprotic ionic liquids[14−18] and has proven very useful for studying proton hopping mechanisms in water,[19,20] metals,[21,22] oxides,[23] and oxo-acid salts.[24] This method has not yet been employed to study proton hopping in ionic liquids.

In this work, we study [Im][TFSI] having a 4:1 ratio of imidazole to HTFSI in order to provide insight into the proton hopping conductivity mechanism. The 3:7 and 1:1 ratios of [Im][TFSI], which are not expected to exhibit proton hopping, are studied for comparison. Given the desire to utilize protic ionic liquids as electrolytes at elevated temperatures, we investigated how the degree of proton hopping, ion aggregation, and the proton transference number vary with temperature. Proton hopping is shown to persist even at 120 °C, leading to a proton transference number of 0.66. We employ QENS to show that hopping is encompassed in the slower of two translational processes, and that this relatively slow process contributes to long-range diffusion more than the faster process. Information about local dynamics is compared to bulk ionic conductivity measurements to provide insight into the effect of proton hopping on macroscopic conductivity.

EXPERIMENTAL SECTION

Ionic Liquid Purification and Preparation. Imidazole (≥95%), d_4-imidazole (≥98% deuteration), and bis-(trifluoromethylsulfonyl)imide (HTFSI, ≥95%) were purchased from Sigma Aldrich (St. Louis, MO) and purified by sublimation under vacuum. The final purity of each starting material was assessed using differential scanning calorimetry (DSC) and ^{1}H NMR (Bruker DRX 500 MHz, Billerica, MA). Purified imidazole or d_4-imidazole and HTFSI were combined in 3:7, 1:1, and 4:1 molar ratios, and the solutions were heated at 100 °C for 2−3 h. The compositions of the resulting [Im][TFSI] and [*d*Im][TFSI] ionic liquids were confirmed by comparing the measured thermal transitions and ^{1}H NMR profiles to literature.[2] Thermal transitions were measured by DSC on a TA Instrument (New Castle, DE) DSC Q20 apparatus to check the purity of the samples. Samples were crimped in an argon atmosphere glovebox using hermetically sealed pans and placed inside a container with desiccant for transfer to the DSC. Indium and dodecane were used as calibration standards. Samples underwent three heating and cooling cycles with a scan rate of 10 °C/min, and thermal transitions from the second heating scan were recorded. The structures of the ionic liquid molecules are shown in Figure 1. Because of their hygroscopic nature, the ionic liquids and their starting materials were handled in an argon atmosphere glovebox and sealed sample holders at all times.

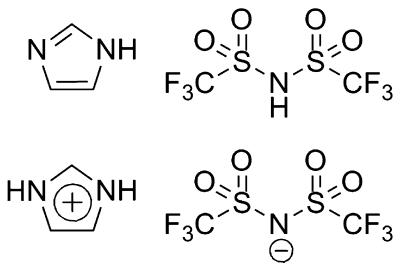

Figure 1. Chemical structures of imidazole, HTFSI, and imidazolium and TFSI ions.

Diffusion Coefficient Measurements. Self-diffusion coefficients of [Im][TFSI] were measured with pulsed-field gradient spin echo (PGSE) and pulsed-field gradient stimulated echo (PGStE) NMR experiments using a Doty Scientific (Columbia, SC) single-axis diffusion probe with temperature control. The applied gradients were calibrated using water[25] and glycerol[26] standards and were found to reach 1.7 T/m. ^{1}H diffusion coefficients were measured in a 7 T superconducting magnet with a 300 MHz Tecmag (Houston, TX) Apollo spectrometer and gradient control, and ^{19}F diffusion coefficients were measured in a 1.5 T superconducting magnet with a 61.2 MHz Tecmag LapNMR spectrometer and gradient control. Experiments were performed between 25 and 120 °C, where the temperature was calibrated[27] using an ethylene glycol standard between 24 and 83 °C and extrapolated to higher temperatures.

The NMR signal attenuation in PGSE and PGStE experiments is described by

$$I = I_0 e^{-D\gamma^2 g^2 \delta^2 (\Delta - \frac{\delta}{3})} \quad (1)$$

where I is the spin−echo signal intensity, I_0 is the signal intensity with zero gradient, γ is the magnetogyric ratio of the probe nucleus, g is the magnitude of the gradient pulse, δ is the duration of the gradient pulse, Δ is the duration of time between the leading edges of the two gradient pulses, and D is the self-diffusion coefficient of the probe nucleus.[26] I was measured as a function of g, and eq 1 was used to determine D. An example plot of I/I_0 as a function of $\gamma^2 g^2 \delta^2 (\Delta - \delta/3)$ is shown in Figure S1 of the Supporting Information. PGSE and

dx.doi.org/10.1021/jp3044237 | J. Phys. Chem. B 2012, 116, 8201−8209

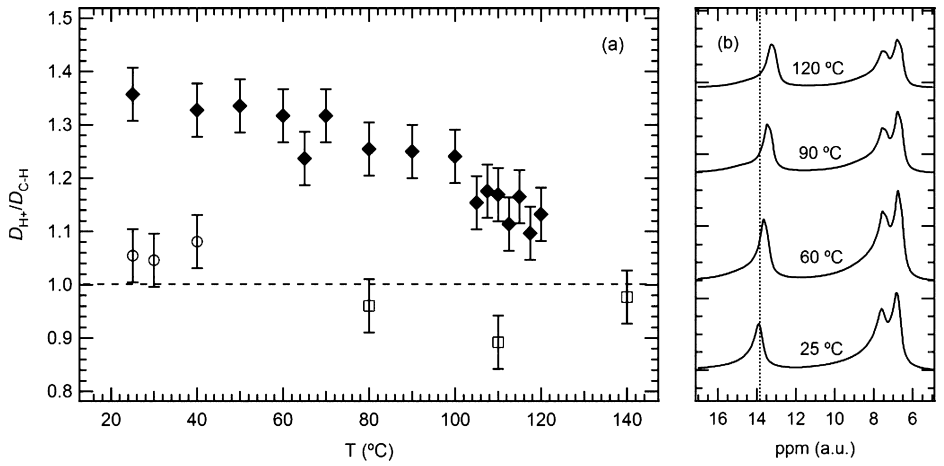

Figure 2. (a) D_{H+}/D_{C-H} as a function of temperature for 4:1 [Im][TFSI] (◆), 1:1 [Im][TFSI] (□), and 3:7 [Im][TFSI] (○). D_{H+}/D_{C-H} is greater than one in 4:1 [Im][TFSI], indicating proton hopping. (b) ^{1}H NMR spectra of 4:1 [Im][TFSI] at various temperatures, derived from PGSE experiments at the lowest gradient strength. The N−H proton peak shifts to lower parts per million at higher temperatures, reflecting changes in the hydrogen bond structure with temperature.

PGStE experiments performed on each sample resulted in consistent measurements of D. Some ^{1}H NMR spectra are reported that were derived from PGSE experiments at the lowest gradient strength.

The diffusion coefficients for protons covalently bound to the carbon atoms on imidazole (C−H protons), D_{C-H}, and protons bound to nitrogen atoms on imidazole (N−H protons), D_{N-H}, were measured separately owing to their chemical shift contrast. The diffusion coefficients of acidic protons, D_{H+}, were calculated according to

$$D_{N-H} = xD_{H+} + (1 - x)D_{C-H} \quad (2)$$

where x is the mole fraction of imidazolium.[2] For ^{19}F experiments, a single peak was observed corresponding to fluorine atoms on the TFSI anion, and a single diffusion coefficient was therefore measured, D_{TFSI}.

Neutron Scattering. Neutron scattering experiments were performed at the National Institute for Standards and Technology (NIST) Center for Neutron Research (NCNR). [Im][TFSI] and [dIm][TFSI] samples were loaded into sample cans with an annular geometry, and the sample transmission was set to about 90% to minimize multiple scattering on both spectrometers. Reduction, visualization, and analysis of data were performed using the DAVE software package developed at NCNR.[28] Fixed window scans (FWS) were performed on the high-flux backscattering spectrometer (HFBS) with an incident neutron wavelength of λ = 6.271 Å and an energy resolution of about 0.8 μeV. Elastic scattering intensity was recorded as the temperature was increased steadily at a rate of 1 K/min from 70 K to a maximum temperature between 360 and 420 K. Data were collected every minute from all 16 detectors, together probing a q range from 0.25 to 1.75 Å^{-1}. The mean-squared displacement of protons as a function of temperature was calculated from the loss of elastic scattering intensity using DAVE. QENS experiments were performed on the HFBS as well as on the disk chopper spectrometer (DCS) at a variety of temperatures that were chosen based on FWS experiments. An incident neutron wavelength of λ = 6 Å and an energy resolution of 64 μeV were used for DCS experiments. Data were binned into nine bins having average q values ranging from 0.35 to 1.8 Å^{-1}, and the data were corrected for empty cell scattering. An incident neutron wavelength of λ = 6.271 Å and an energy resolution of about 0.8 μeV were used for HFBS experiments. Data from all 16 detectors were used to probe a q range from 0.25 to 1.75 Å^{-1}. The acquired data were corrected for detector efficiencies (determined using a vanadium standard), and the resolution functions of the instruments were determined by measuring scattering from 4:1 [dIm][TFSI] at 35 K (on the DCS) and 4:1 [Im][TFSI] at 30 K (on the HFBS) where all the signals are expected to be from elastic scattering.

Ionic Conductivity Measurements. Bulk ionic conductivity was measured using two-point probe through-plane AC impedance spectroscopy. An annular ionic liquid-containing spacer was placed between two stainless steel electrodes. The spacers were made from Kapton or Teflon and had thicknesses ranging from 25 μm to 0.3 cm and inner diameters ranging from 0.3 to 0.7 cm. The samples were then placed in homemade, airtight stainless steel cells with Teflon flanges. The cells were screwed together in the glovebox, clamped to maintain constant pressure in an oven outside the glovebox, and heated at the maximum measurement temperature for 12 h before measurements were made. Impedance measurements were performed using a Gamry (Philadelphia, PA) Reference 600 Potentiostat at descending temperatures. An alternating current signal with an amplitude of 5 mV was applied in the frequency range of 100−65000 Hz. The non-zero x intercept in the Nyquist plot of the negative-imaginary part of the impedance versus the real part of the impedance was taken as the sample resistance, R. The ionic conductivity, σ, was calculated as t/AR, where t and A are the thickness and area of the sample, respectively.

RESULTS AND DISCUSSION

Comparing D_{H+} to D_{C-H} provides a quantitative description of how proton hopping increases proton transport vis-à-vis vehicle diffusion alone (Figure 2a). A ratio of approximately unity is expected and observed in cases where there is no excess imidazole to act as a proton acceptor (3:7 and 1:1 [Im][TFSI]). Also as expected, this ratio is greater than one in 4:1 [Im][TFSI] (D_{H+}/D_{C-H} = 1.36 at 25 °C, in close agreement with previous work[2]). Proton hopping decreases with increasing temperature but persists over the entire experimental temperature range; D_{H+}/D_{C-H} decreases to

dx.doi.org/10.1021/jp3044237 | J. Phys. Chem. B 2012, 116, 8201−8209

about 1.1 at 120 °C. Since proton hopping relies on hydrogen bonding between imidazole molecules,[4,7−10] it is expected that the decrease in proton hopping at elevated temperatures is related to a number of changes that occur in the imidazole hydrogen bond structure with increased temperature. These include an increased hydrogen bond length, shortened average lifetime, or decreased number of hydrogen bonds.[29,30] The latter two effects are also related to an increase in the rate of imidazole ring flipping observed with increasing temperature.[11−13] Figure 2b shows how the NMR spectrum of 4:1 [Im][TFSI] evolves with increasing temperature. The peak that corresponds to N−H protons, which is farthest downfield, shifts upfield with increasing temperature. This peak shift reflects the overall increased electron density surrounding the nuclei of the N−H protons that accompanies the changes in hydrogen bond structure.[2]

The relationship between hydrogen bond character and proton transport is complex because proton hopping relies on the existence of hydrogen bonds as well as the ability of hydrogen bonds within the network to break and re-form.[4,7−10] Proton diffusion enhancement due to the analogous Grotthuss mechanism in water increases with increasing temperature between about 0 and 150 °C and decreases at higher temperatures; hydrogen bond reconstruction is the limiting process at low temperatures, whereas the diminished extent of hydrogen bonding is the limiting factor at high temperatures.[31,32] In contrast, proton hopping in 4:1 [Im][TFSI] decreases monotonically with increasing temperature between 25 and 120 °C, implying that the overall weakening of the hydrogen bond network is the limiting factor for proton hopping in this entire temperature range.

QENS experiments provide more details about proton dynamics in [Im][TFSI]. The relatively large incoherent neutron scattering cross section of ^{1}H compared to other atoms leads to the selective observation of self-correlated hydrogen motion in QENS experiments, making QENS an ideal tool for studying proton-transport mechanisms. Ionic liquids synthesized from deuterated imidazole were used for QENS experiments in order to selectively observe acidic proton dynamics, although some exchange between acidic protons and N−H protons was expected to occur. Fixed window scans (FWS) were performed on the HFBS first, to ascertain how the proton dynamics are affected by thermal transitions in all the samples including pure d_4-imidazole and HTFSI. The mean-squared displacements of protons, $\langle u^2(T)\rangle$, were calculated from FWS experiments using the following expression relating $\langle u^2(T)\rangle$ to the elastic scattering intensity, $I(q,T)$:

$$I(q, T) = \exp\left[-\frac{q^2\langle u^2(T)\rangle}{3}\right] \quad (3)$$

Equation 3 makes use of the Gaussian approximation, which presumes that the distribution of particle displacements at long times is Gaussian as it would be in a system made up of harmonic oscillators in thermal equilibrium.[33] Figure 3 shows $\langle u^2(T)\rangle$ as a function of temperature for 3:7 and 4:1 [dIm][TFSI]. At the lowest temperatures, the mean-squared displacements of the two ionic liquids are similar and increase slowly and linearly with temperature, consistent with the Debye−Waller factor. The mean-squared displacements begin to diverge near the known[2] glass transition temperature, T_g, of each ionic liquid. The observed crystallization and melting temperatures of each ionic liquid, T_c and T_m, respectively, agree

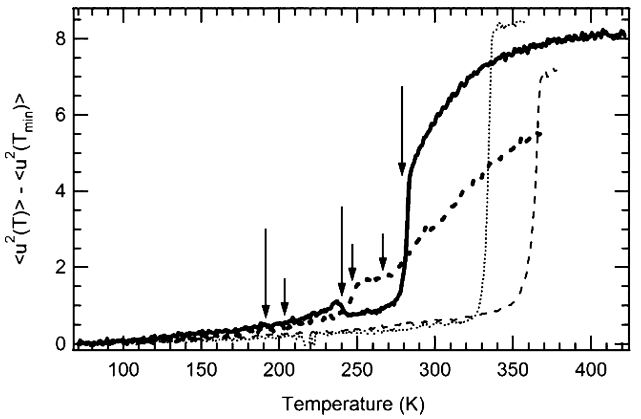

Figure 3. Mean-squared displacement of protons as a function of temperature for 3:7 [dIm][TFSI] (thick dashed line), 4:1 [dIm][TFSI] (thick solid line), d_4-imidazole (thin dashed line), and HTFSI (thin dotted line). T_g, T_c, and T_m from ref 2 are indicated with short and long arrows for 3:7 and 4:1 [dIm][TFSI], respectively, where the transitions increase in temperature in the order $T_g < T_c < T_m$.

well with DSC experiments.[2] QENS experiments on the HFBS were performed above the T_m of each ionic liquid in the temperature regimes where the mean-squared displacements increase steadily with temperature. Higher temperatures could be probed using the DCS because it measures higher-energy scattering corresponding to faster motions. QENS experiments were also performed on 4:1 [dIm][TFSI] between T_c and T_m by cooling the sample from above T_m. (QENS data at all temperatures are shown in Figures 6 and 7.) For comparison, the mean-squared displacements of d_4-imidazole and HTFSI are also shown in Figure 3. The much sharper transitions at T_m and the plateaus in mean-squared displacements above T_m indicate truly first-order transitions. Therefore, quasi-elastic scattering for these compounds above the transition temperatures is too high in energy to be measured by QENS experiments on the HFBS.

QENS experiments were performed using both the DCS and HFBS to probe proton dynamics over a wide energy range. Representative HFBS scattering profiles are shown in Figure 4. As the scattering vector q increases, the full-width at half-maximum (fwhm) of quasi-elastic scattering increases, indicating translational motion processes in each energy range. Quasi-elastic scattering was modeled to quantify its q dependence, and example fits are shown in Figure 5. Similar scattering profiles and fits were obtained for DCS data, and examples are shown in Figures S2 and S3 of the Supporting Information. Two Lorentzian functions were used to fully capture the scattering profiles, consistent with previous QENS studies of ionic liquids above T_m.[14,16] In the case of DCS profiles, one Lorentzian describes the main quasi-elastic scattering contribution, and one describes the high-energy background signal. In the case of HFBS profiles, lower-energy processes are resolved compared to DCS profiles. One Lorentzian describes the main quasi-elastic scattering contribution in this energy range, and the second, broader Lorentzian is the same as the main Lorentzian in the DCS energy range.

The q dependence of the fwhm of the quasi-elastic scattering contributions, Γ, provides information regarding the mechanism of translational proton motion. When diffusion is purely Fickian, Γ is expected to vary linearly with q^2 according to[34]

dx.doi.org/10.1021/jp3044237 | J. Phys. Chem. B 2012, 116, 8201−8209

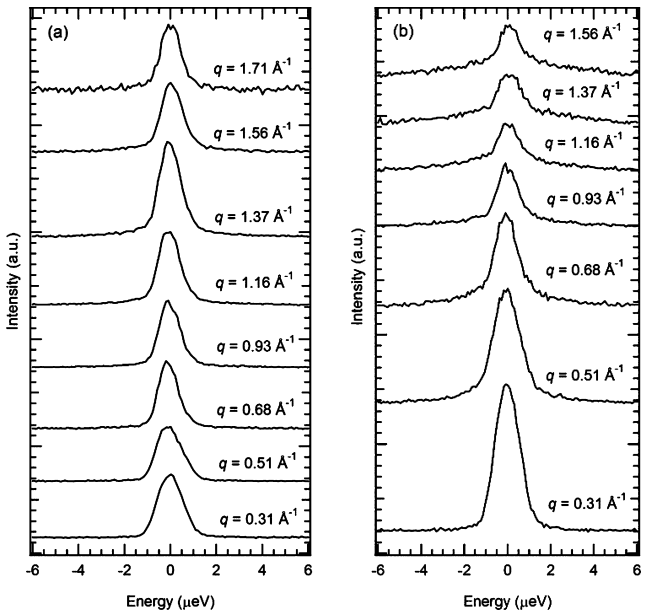

Figure 4. Example HFBS QENS scattering profiles of (a) 3:7 [*d*Im][TFSI] and (b) 4:1 [*d*Im][TFSI], at 290 K. The full width at half-maximum (fwhm) of quasi-elastic scattering increases with increasing q, indicating translational motion processes.

$$\frac{\Gamma}{2} = \hbar D q^2 \tag{4}$$

Equation 4 adequately describes simple liquids such as argon[35] and even some more complex liquids such as the ionic liquid 1-butyl-3-methylimidazolium:chloride.[15] When molecular interactions are significant, for instance in the case of the ionic liquids 1-ethyl-3-methylimidazolium:bromide[14] and *N,N,N′,N′*-tetramethylguanidinium:bis(perfluoroethylsulfonyl)imide ($[H_2NC(dma)_2][BETI]$),[16] deviations from eq 4 are observed at high values of q corresponding to length scales smaller than the interaction distance. In these cases, the Jump-Diffusion model[36] is often used to describe the variation of Γ with q^2 as

$$\frac{\Gamma}{2} = \frac{\hbar D q^2}{1 + D q^2 \tau_0} \tag{5}$$

where τ_0 is the residence time between jumps, or the molecular interaction time. Furthermore, the Jump-Diffusion model describes the complex dynamics of protons in supercooled water, which are dominated by Grotthuss proton transfer between water molecules through hydrogen bonds.[19,20] In this case, τ_0 is the time between proton transfer events.

The FWHMs of the Lorentzians describing the main quasi-elastic scattering contributions to DCS and HFBS scattering profiles for 3:7 and 4:1 [*d*Im][TFSI] are plotted as a function of q^2 in Figures 6 and 7 at all experimental temperatures. (The high-energy background signal in DCS has very little q or temperature dependence.) On the basis of the complex diffusion observed previously in ionic liquids and water, it is unsurprising that the data for both ionic liquids deviate from linear behavior and are described well by eq 5. The nonlinearity probably reflects a combination of strong molecular interactions and proton hopping in the case of 4:1 [*d*Im][TFSI].

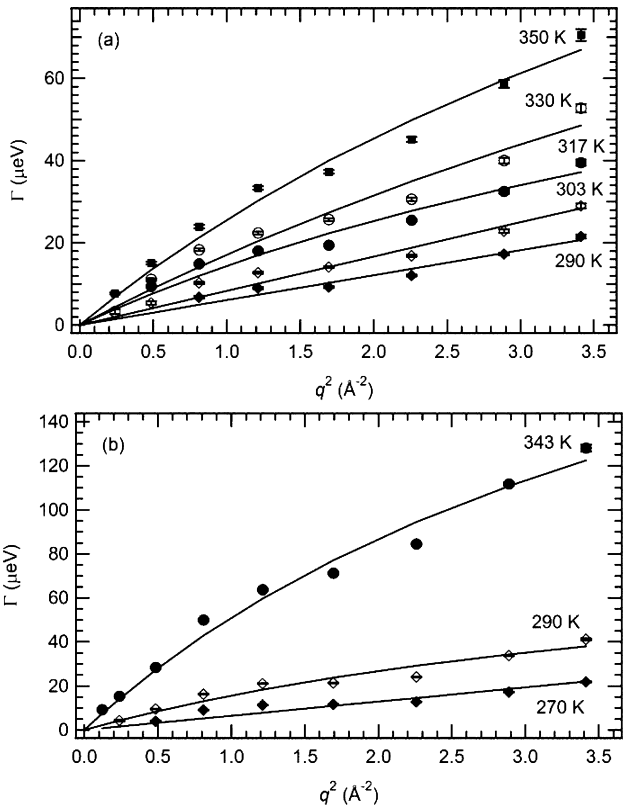

Figure 6. Γ of the main Lorentzian peak fit to the DCS QENS signal as a function of q^2 for (a) 3:7 [*d*Im][TFSI] and (b) 4:1 [*d*Im][TFSI], at various temperatures. Error bars represent one standard deviation of the Lorentzian fits. Solid curves are fits to the data using eq 5.

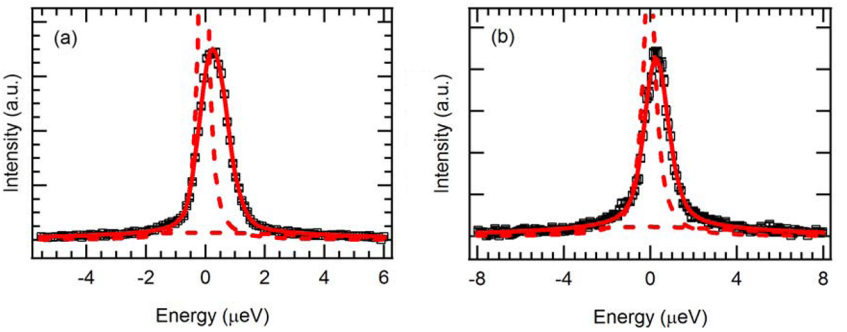

Figure 5. Representative HFBS QENS profiles of (a) 3:7 [*d*Im][TFSI] at T = 290 K and q = 1.16 Å^{-1} and (b) 4:1 [*d*Im][TFSI] at T = 270 K and q = 0.99 Å^{-1}. The solid lines are the total fits to the data, while the dashed lines are the component fits (two Lorentzian functions).

dx.doi.org/10.1021/jp3044237 | J. Phys. Chem. B 2012, 116, 8201−8209

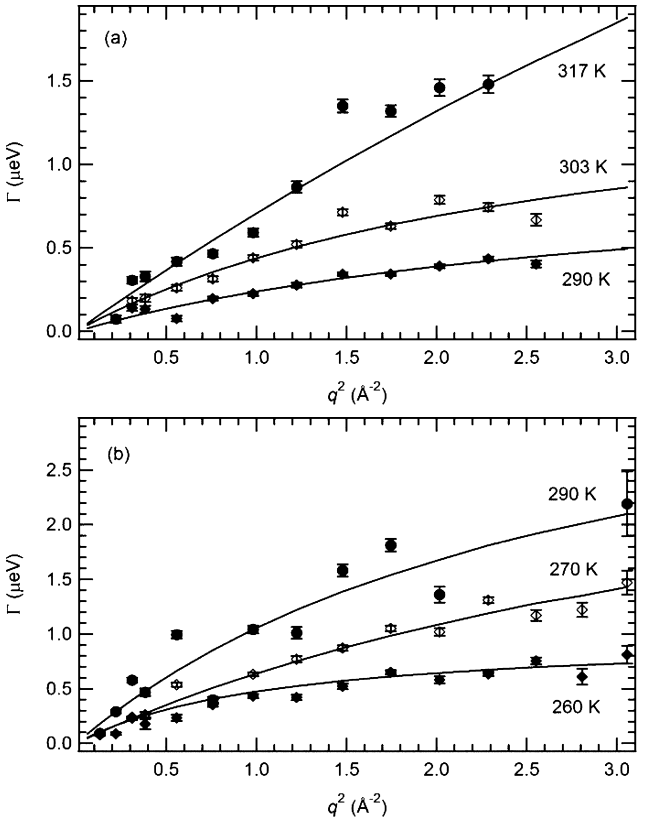

Figure 7. Γ of the main Lorentzian peak fit to the HFBS QENS signal as a function of q^2 for (a) 3:7 [*d*Im][TFSI] and (b) 4:1 [*d*Im][TFSI], at various temperatures. Error bars represent one standard deviation of the Lorentzian fits. Solid curves are fits to the data using eq 5.

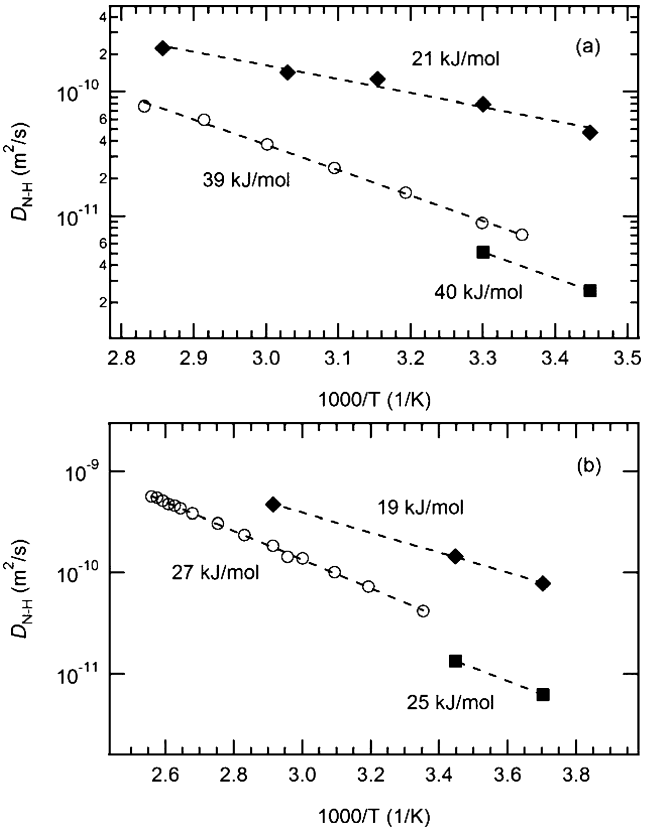

Figure 8. D_{N-H} measured with NMR (○) compared to *D* calculated from DCS (◆) and HFBS (■) measurements for (a) 3:7 [*d*Im][TFSI] and (b) 4:1 [*d*Im][TFSI]. Arrhenius fits are shown with dashed lines, and activation energies determined by the fits are labeled.

It is interesting that there are two distinct contributions to translational motion with different characteristic energies, one in the main energy range of the DCS and one in the main energy range of the HFBS. The diffusion coefficients associated with each process were estimated from the fits of eq 5 to the data and are plotted in Figure 8 as a function of temperature along with D_{N-H} measured by NMR. D_{N-H} falls between the diffusion coefficients associated with each process identified by QENS, confirming that both contribute to long-range proton diffusion. The lower-energy diffusion process (in the main energy range of HFBS) is the slower of the two. These data points fall closest to D_{N-H} and have activation energies more similar to D_{N-H}, indicating that protons participating in the slower process contribute more to long-range N−H proton diffusion than those participating in the faster process. This suggests that either the faster diffusion process is spatially restricted or a greater population of N−H protons is able to participate in the slower diffusion process. Comparing the areas of the Lorentzians associated with each diffusion process in the HFBS scattering profiles confirms that both phenomena play a role. At low temperatures, the fraction of protons participating in the faster process is significantly smaller than the fraction participating in the slower process (Figure 9). In addition, the number of protons participating in the faster process increases with increasing *q*, especially at high temperatures. This is indicative of a spatially confined process on the length scale of angstroms.

Two translational diffusion processes have also been observed previously in the protic ionic liquid [H_2NC(dma)$_2$][BETI], where the faster process was attributed to the motion of ions in structurally well-defined clusters with an associated length scale of 8 Å.[16] Such clusters have been observed in imidazolium-based ionic liquids experimentally[37−40] and theoretically.[41−43] It is likely that this type of spatial heterogeneity also explains the existence of two translational diffusion processes in [*d*Im][TFSI]. In the case of [H_2NC(dma)$_2$][BETI], the spatial confinement of the fast process was evidenced by a low *q* (q^2 < 0.25 Å^{-2}) plateau in the fwhm of the higher-energy quasi-elastic signal. No such plateau is observed for [*d*Im][TFSI] in Figure 6, but reliable DCS data below q^2 = 0.24 were not obtained.

The energetics of proton hopping are illuminated by comparing the proton dynamics of 4:1 [*d*Im][TFSI] and [Im][TFSI]. The quasi-elastic signal is more affected by proton hopping in the deuterated ionic liquid, which contains only N−H protons that come from HTFSI, than in the hydrogenated ionic liquid, which contains C−H and N−H protons. Figure 10 shows Γ versus q^2 from DCS and HFBS experiments on both samples at 290 K. There is a much greater discrepancy between the HFBS data for the hydrogenated and deuterated ionic liquids than between the DCS data sets, implying that proton hopping is mostly contained in the slower, unconfined process that contributes to long-range proton diffusion more than the faster process. This result is reasonable since it is clear that proton hopping strongly influences long-range proton diffusion.[2,3] While the Γ versus q^2 data for both 4:1 [*d*Im][TFSI] and [Im][TFSI] demonstrate nonlinear behavior,

dx.doi.org/10.1021/jp3044237 | J. Phys. Chem. B 2012, 116, 8201−8209

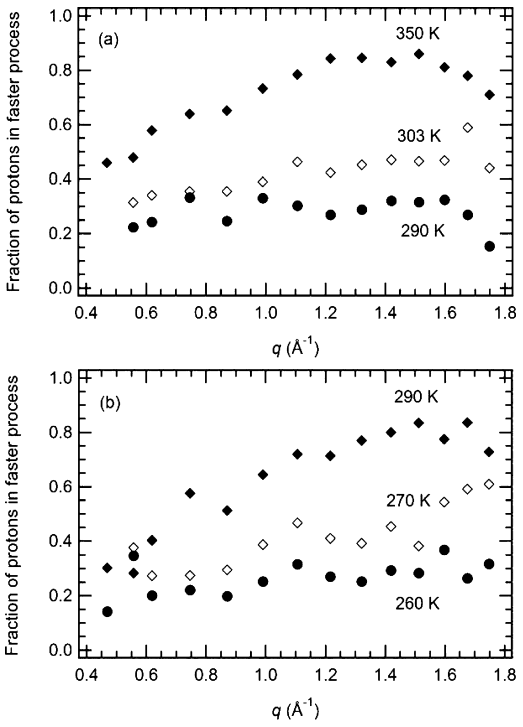

Figure 9. Fraction of quasi-elastic scattering due to proton participation in a faster, high-energy process as a function of q for (a) 3:7 [*d*Im][TFSI] and (b) 4:1 [*d*Im][TFSI], at various temperatures. The fractions were determined by comparing the peak areas of each Lorentzian in HFBS scattering profiles.

the data for the deuterated ionic liquid clearly exhibit a greater deviation from linearity due to proton hopping.

To the best of our knowledge, this is the first time that the proton hopping mechanism in imidazole has been observed by QENS. It is expected that with an improved signal-to-noise ratio, in combination with more sophisticated mathematical models and numerical simulation, future QENS experiments could quantify the degree of proton hopping and characterize important hopping parameters, including hop distance, time scale for proton hopping and imidazole reorientation, and activation energy for hops. This not only would be useful for providing insight into proton-transport mechanisms in ionic liquids but also would be invaluable for evaluating ionic liquid-containing membranes of interest for electrochemical applications.[44]

As a result of proton hopping, 4:1 [Im][TFSI] achieves greater proton transport as well as a higher proton transference number than the ionic liquids without excess imidazole. As shown in Figure 11, molecular diffusion is already greatest in 4:1 [Im][TFSI], most likely because it has the lowest T_g (T_g = −81 °C, compared to T_g = −68 °C for 3:7 [Im][TFSI] and T_m = 73 °C for 1:1 [Im][TFSI], which does not have a measurable T_g).[2] D_{H+} is further enhanced as a result of proton hopping. Furthermore, since proton transport becomes somewhat decoupled from simple vehicle diffusion of imidazolium cations, the proton transference number is high, ranging between 0.66 and 0.78 in the experimental temperature range. The transference numbers were calculated as

$$\frac{D_{H+}}{D_{H+} + D_{TFSI}} \quad (6)$$

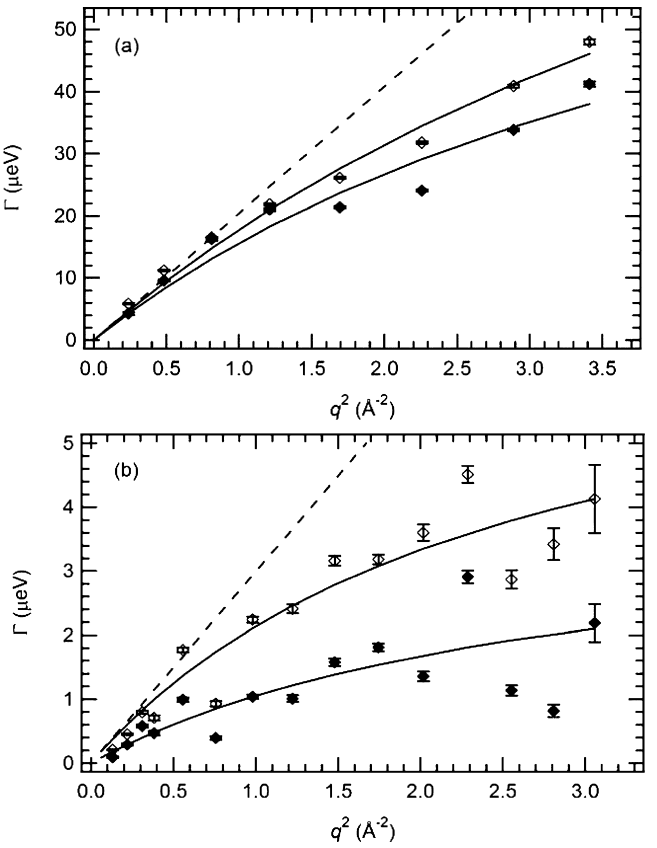

Figure 10. Γ of the main Lorentzian peak fit to the (a) DCS and (b) HFBS QENS signals as a function of q^2 for 4:1 [*d*Im][TFSI] (closed symbols) and 4:1 [Im][TFSI] (open symbols) at 290 K. Error bars represent one standard deviation of the Lorentzian fits. Solid curves are fits to the data using eq 5. Dashed curves are Fickian diffusion curves (eq 4) using the diffusion coefficients derived from fits of eq 5 to 4:1 [*d*Im][TFSI] data.

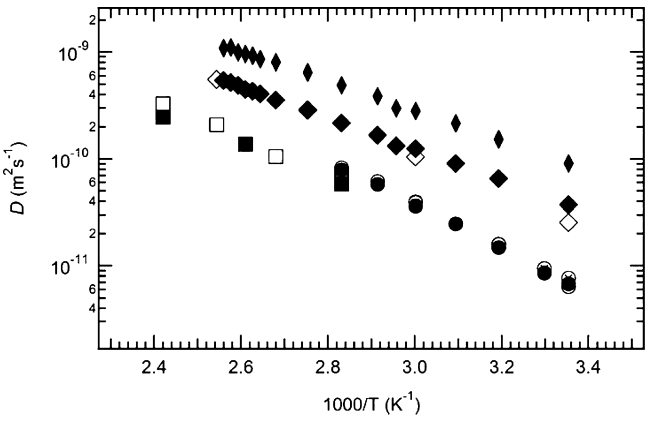

Figure 11. D_{C-H} (closed symbols) and D_{TFSI} (open symbols) for 4:1 [Im][TFSI] (diamonds), 1:1 [Im][TFSI] (squares), and 3:7 [Im][TFSI] (circles). For 3:7 [Im][TFSI], D_{TFSI} was measured by ^{19}F and ^{1}H (circles marked with X) NMR. D_{H+} values for 4:1 [Im][TFSI] are represented by narrow closed diamonds.

Without proton hopping, the transference number would be much closer to 0.50 since D_{C-H} and D_{TFSI} are very similar.

In addition to having high proton diffusion and a high proton transference number, there is very little ion aggregation in 4:1 [Im][TFSI], allowing very high ionic conductivity to be achieved. The degree of ion aggregation is estimated by

dx.doi.org/10.1021/jp3044237 | J. Phys. Chem. B 2012, 116, 8201−8209

comparing the measured bulk ionic conductivity to that predicted by the ion-diffusion coefficients measured by NMR and the Nernst–Einstein equation:

$$\sigma = \frac{F^2}{RT}(c_{m,H+}D_{H+} + c_{m,TFSI}D_{TFSI}) \quad (7)$$

where $c_{m,H+}$ and $c_{m,TFSI}$ are the molar concentrations of acidic protons and TFSI anions, respectively. The predicted conductivity of 4:1 [Im][TFSI] is very close to the actual conductivity (Figure 12), indicating that there is very little ion

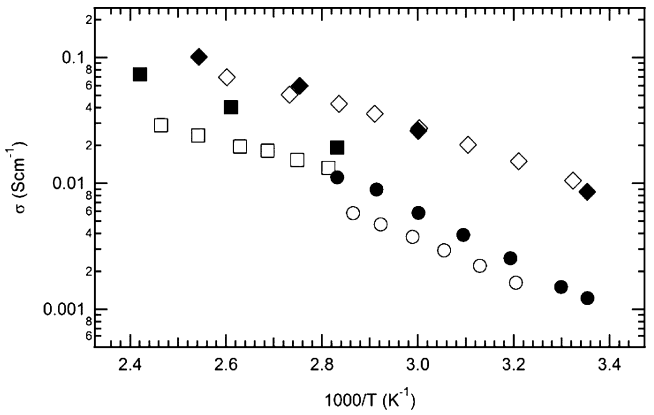

Figure 12. Measured σ (open symbols) and σ calculated from NMR diffusion coefficients and Nernst–Einstein equation (closed symbols) for 4:1 [Im][TFSI] (diamonds), 1:1 [Im][TFSI] (squares), and 3:7 [Im][TFSI] (circles). Measured σ is in good agreement with previously reported measurements.[2]

aggregation. In contrast, ion aggregation in 3:7 and 1:1 [Im][TFSI] causes the ionic conductivity to be lower than that predicted by eq 7.

CONCLUSION

Proton transport in [Im][TFSI] ionic liquids was investigated using NMR and QENS, with specific focus on the proton hopping mechanism that occurs when the ionic liquid contains excess imidazole. Proton hopping was found to decrease with increasing temperature, but significant proton hopping exists even at the maximum experimental temperature of 120 °C. This, in combination with minimal ion aggregation, leads to high proton conductivity over a wide temperature range. Furthermore, proton hopping results in a partial decoupling of proton transport from imidazole diffusion, which leads to a high proton transference number.

Proton hopping was shown to be characterized by a deviation from a linear Γ versus q^2 relationship in QENS experiments, opening the door for future QENS studies of proton hopping in ionic liquids and ionic-liquid composite materials. In addition, two contributions to translational diffusion were identified. Proton hopping is mostly encompassed in the slower, lower-energy process, which contributes to long-range proton diffusion more than the faster process.

ASSOCIATED CONTENT

Supporting Information

Representative PGSE NMR data as well as representative DCS QENS scattering profiles and fits. This material is available free of charge via the Internet at http://pubs.acs.org.

AUTHOR INFORMATION

Corresponding Author

*E-mail: mhoarfrost@berkeley.edu.

Notes

The authors declare no competing financial interest.

ACKNOWLEDGMENTS

This material is based on work performed by the Joint Center for Artificial Photosynthesis, a DOE Energy Innovation Hub, as follows: Material preparation and investigation of ionic liquid dynamics was supported by the Assistant Secretary for Energy Efficiency and Renewable Energy, Office of Hydrogen, Fuel Cell, and Infrastructure Technologies of the U.S. Department of Energy under Contract DE-AC02-05CH11231. Continued investigation of ionic-liquid dynamics and interpretation of dynamical data was supported through the Office of Science of the U.S. Department of Energy under Grant DE-SC0004993. M.L.H. is thankful for support from an NSF Graduate Research Fellowship. This work utilized facilities at the NIST Center for Neutron Research (NCNR) supported in part by the National Science Foundation under Grant DMR-0944772. We gratefully acknowledge Dr. Timothy Jenkins and Dr. Craig Brown for experimental assistance at the NCNR as well as Dr. Joel Stettler for technical assistance with NMR experiments. This report was prepared as an account of work sponsored by an agency of the United States Government. Neither the United States Government nor any agency thereof, nor any of its employees, makes any warranty, express or implied, or assumes any legal liability or responsibility for the accuracy, completeness, or usefulness of any information, apparatus, product, or process disclosed, or represents that its use would not infringe upon privately owned rights. Reference herein to any specific commercial product, process, or service by trade name, trademark, manufacturer, or otherwise does not necessarily constitute or imply its endorsement, recommendation, or favoring by the United States Government or any agency thereof. The views and opinions of authors expressed herein do not necessarily state or reflect those of the United States Government or any agency thereof.

REFERENCES

(1) Ohno, H. *Electrochemical Aspects of Ionic Liquids*; Wiley-Interscience: New York, 2005.
(2) Noda, A.; Susan, A. B.; Kudo, K.; Mitsushima, S.; Hayamizu, K.; Watanabe, M. *J. Phys. Chem. B* **2003**, *107* (17), 4024–4033.
(3) Kreuer, K. D.; Fuchs, A.; Ise, M.; Spaeth, M.; Maier, J. *Electrochim. Acta* **1998**, *43* (10–11), 1281–1288.
(4) Munch, W.; Kreuer, K. D.; Silvestri, W.; Maier, J.; Seifert, G. *Solid State Ionics* **2001**, *145* (1–4), 437–443.
(5) Ueki, T.; Watanabe, M. *Macromolecules* **2008**, *41* (11), 3739–3749.
(6) Riehl, N. *Trans. N.Y. Acad. Sci.* **1965**, *27* (7), 772–781.
(7) Chen, H.; Yan, T. Y.; Voth, G. A. *J. Phys. Chem. A* **2009**, *113* (16), 4507–4517.
(8) Iannuzzi, M. *J. Chem. Phys.* **2006**, *124*, 20.
(9) Iannuzzi, M.; Parrinello, M. *Phys. Rev. Lett.* **2004**, *93*, 2.
(10) Yan, S. H.; Bu, Y. X.; Cao, Z. H.; Li, P. *J. Phys. Chem. A* **2004**, *108* (34), 7038–7049.
(11) Daycock, J. T.; Jones, G. P.; Evans, J. R. N.; Thomas, J. M. *Nature* **1968**, *218* (5142), 672–673.
(12) Goward, G. R.; Saalwachter, K.; Fischbach, I.; Spiess, H. W. *Solid State Nucl. Magn. Reson.* **2003**, *24* (2–3), 150–162.
(13) Fischbach, I.; Spiess, H. W.; Saalwachter, K.; Goward, G. R. *J. Phys. Chem. B* **2004**, *108* (48), 18500–18508.

(14) Aoun, B.; Gonzalez, M. A.; Ollivier, J.; Russina, M.; Izaola, Z.; Price, D. L.; Saboungi, M. L. *J. Phys. Chem. Lett.* **2010**, *1* (17), 2503−2507.
(15) Inamura, Y.; Yamamuro, O.; Hayashi, S.; Hamaguchi, H. O. *Phys. B (Amsterdam, Neth.)* **2006**, *385*, 732−734.
(16) Mamontov, E.; Luo, H. M.; Dai, S. *J. Phys. Chem. B* **2009**, *113* (1), 159−169.
(17) Triolo, A.; Russina, O.; Arrighi, V.; Juranyi, F.; Janssen, S.; Gordon, C. M. *J. Chem. Phys.* **2003**, *119* (16), 8549−8557.
(18) Triolo, A.; Russina, O.; Hardacre, C.; Nieuwenhuyzen, M.; Gonzalez, M. A.; Grimm, H. *J. Phys. Chem. B* **2005**, *109* (46), 22061−22066.
(19) Chen, S. H.; Teixeira, J.; Nicklow, R. *Phys. Rev. A* **1982**, *26* (6), 3477−3482.
(20) Teixeira, J.; Bellissentfunel, M. C.; Chen, S. H.; Dianoux, A. J. *Phys. Rev. A* **1985**, *31* (3), 1913−1917.
(21) Skold, K.; Nelin, G. *J. Phys. Chem. Solids* **1967**, *28* (12), 2369−2380.
(22) Rowe, J. M.; Skold, K.; Flotow, H. E.; Rush, J. J. *J. Phys. Chem. Solids* **1971**, *32* (1), 41−54.
(23) Hempelmann, R.; Karmonik, C.; Matzke, T.; Cappadonia, M.; Stimming, U.; Springer, T.; Adams, M. A. *Solid State Ionics* **1995**, *77*, 152−156.
(24) Ishikawa, A.; Maekawa, H.; Yamamura, T.; Kawakita, Y.; Shibata, K.; Kawai, M. *Solid State Ionics* **2008**, *179* (40), 2345−2349.
(25) Price, W. S. *Concepts Magn. Reson.* **1998**, *10* (4), 197−237.
(26) Stejskal, E. O.; Tanner, J. E. *J. Chem. Phys.* **1965**, *42* (1), 288−292.
(27) Raiford, D. S.; Fisk, C. L.; Becker, E. D. *Anal. Chem.* **1979**, *51* (12), 2050−2051.
(28) Azuah, R. T.; Kneller, L. R.; Qiu, Y. M.; Tregenna-Piggott, P. L. W.; Brown, C. M.; Copley, J. R. D.; Dimeo, R. M. *J. Res. Natl. Inst. Stand. Technol.* **2009**, *114* (6), 341−358.
(29) Cavalcanti, W. L.; Portaluppi, D. F.; Joswig, J. O. *J. Chem. Phys.* **2010**, *133*, 10.
(30) Kanaskov, Yd.; Sukhoruk, Bi.; Pentin, Y. A.; Komarovs, Gv. *Izv. Akad. Nauk SSSR, Ser. Khim.* **1970**, *8*, 1735.
(31) Gierer, A.; Wirtz, K. *J. Chem. Phys.* **1949**, *17* (8), 745−746.
(32) Gileadi, E.; Kirowa-Eisner, E. *Electrochim. Acta* **2006**, *51* (27), 6003−6011.
(33) Zorn, R. *Nucl. Instrum. Methods Phys. Res., Sect. A* **2007**, *572* (2), 874−881.
(34) Bée, M. *Quasielastic Neutron Scattering: Principles and Applications in Solid State Chemistry, Biology and Materials Science*; Taylor & Francis, 1988.
(35) Dasannacharya, B. A.; Rao, K. R. *Phys. Rev.* **1965**, *137* (2A), A417−A427.
(36) Chudley, C. T.; Elliott, R. J. *Proc. Phys. Soc., London* **1961**, *77* (494), 353−361.
(37) AbdulSada, A. K.; Elaiwi, A. E.; Greenway, A. M.; Seddon, K. R. *Eur. Mass Spectrom.* **1997**, *3* (3), 245−247.
(38) Dupont, J. *J. Braz. Chem. Soc.* **2004**, *15* (3), 341−350.
(39) Gozzo, F. C.; Santos, L. S.; Augusti, R.; Consorti, C. S.; Dupont, J.; Eberlin, M. N. *Chem.—Eur. J.* **2004**, *10* (23), 6187−6193.
(40) Kuang, Q. L.; Zhang, J.; Wang, Z. G. *J. Phys. Chem. B* **2007**, *111* (33), 9858−9863.
(41) Del Popolo, M. G.; Voth, G. A. *J. Phys. Chem. B* **2004**, *108* (5), 1744−1752.
(42) Habasaki, J.; Ngai, K. L. *J. Chem. Phys.* **2008**, *129*, 19.
(43) Morrow, T. I.; Maginn, E. J. *J. Phys. Chem. B* **2002**, *106* (49), 12807−12813.
(44) Hoarfrost, M. L.; Tyagi, M. S.; Segalman, R. A.; Reimer, J. A. *Macromolecules* **2012**, *45* (7), 3112−3120.